Subproject B3.4

Control of Quantum Information Circuits

Principle Investigators: Alexey V. Ustinov and Michael Siegel

CFN-Financed Scientists: Markus Jerger (0.5 E13, 13.5 months),
Fedorov Kirill (0.5 E13, 1.5 months),
Tobias Wirth (0.75 E13, 1 months),
Stefan Wünsch (1 E13, 18 months)

Further Scientists: Dr. Konstantin Il'in, Gerd Hammer, Erich Crocoll, Ch. Kaiser,
Dr. Stefano Poletto

Physikalisches Institut
Karlsruhe Institute of Technology

Institut für Mikro- und Nanoelektronische Systeme
Karlsruhe Institute of Technologyemeinschaft

Control of Quantum Information Circuits

Introduction and Summary

Quantum computation is expected to be the next big leap forward in information processing. A number of problems that are computationally very expensive on classical computers, requiring factorial time, can be solved in polynomial time on quantum computers. Instead of operating on a single number represented as a stream of bits that can be zero or one, quantum computers operate on qubits holding a superposition of zero and one, effectively performing a calculation on all representable numbers simultaneously.

The workhorses of subproject B3.4 are superconducting qubits. These qubits are among the most promising candidates for scalable quantum computers, because they can be manufactured lithographically with custom parameters. They can also be integrated into additional circuitry designed to manipulate, measure (readout) and transfer their quantum state.

Previous implementations lack scalability, because the conventionally used SQUID readout requires dedicated external circuitry and wiring for each additional qubit. Multiplexing readout of two and three qubits through the same line has been demonstrated, but the scheme used also does not scale to a larger number of devices. Thus, the first aim of subproject B3.4 was the development of a multiplexing readout scheme that had the potential to address a large number of devices through a single line.

Instead of a switching current measurement, the state of a single qubit can also be measured by observing the dispersive shift of the frequency of a resonant circuit coupled to the qubit. Apart from the fact that this readout has lower back-action on the qubit, it is also well suited for frequency-division multiplexing, because the readout channels of multiple qubits can simply be designed to be at different points in frequency space and be combined onto a single high-frequency transmission line.

Members of subproject B3.4 have implemented the readout of a single Josephson phase qubit through a SQUID resonator coupled to the qubit [B3.4:1], and explored the intermediate coupling regime between a Josephson flux qubit and a resonator [B3.4:2], where back-action is further reduced. The number of devices that can be read out simultaneously scales linearly with the available detection bandwidth, which makes wide-band cryogenic amplifiers necessary [B3.4:3].

Simultaneous frequency-division multiplexing readout was experimentally demonstrated with an array of three microwave kinetic inductance detectors [B3.4:4], using a scheme compatible with multiplexing qubit readout. Recently, we showed multiplexing readout of 7 Josephson flux qubits through a single line [B3.4:5].

In the second half of the project run-time, the focus will be on devices with multiple interacting qubits, each coupled to its individual readout resonator, which will enable the execution of multi-qubit algorithms on the qubit register.

1. Readout of Superconducting Qubits through Resonators

One of the key ingredients in quantum information circuits is an effective means of retrieving the result of a computation from the system, encoded in the quantum states of the qubits. The quantum
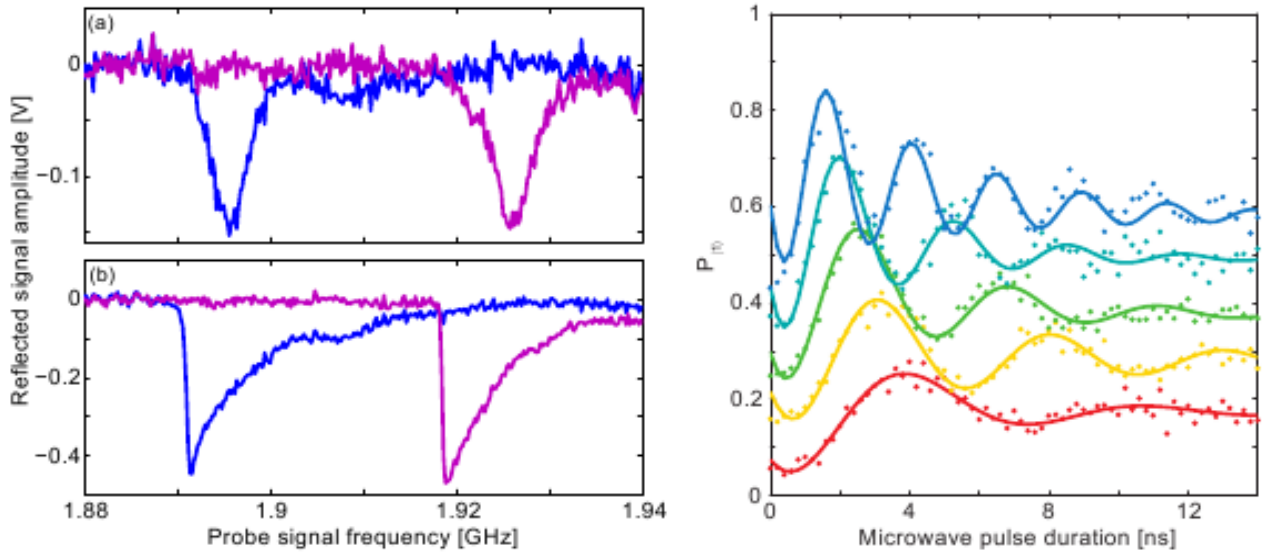
Fig. 1: (left) Shift of the resonance frequency of the SQUID resonator due to the qubit changing its state in thelinear (a) and non-linear (b) regime. (right) Coherent oscillations of the qubit for different driving powers. Curves are offset by 0.1 for better visibility.

state of flux andphase qubits can be distinguished by the magnetic flux threading thequbit loop, which can be detected with a dc SQUID coupled to the qubit.The conventional method to read out the qubit is to record the biascurrent at which the SQUID switches to its non-superconducting state.This creates heat directly on the chip and generates quasiparticlesin the circuit, which makes a relatively long cool down time of 1-2msnecessary before the experiment can be repeated. If many qubits wereread out simultaneously, a substantially longer cool down time would be required.

We developed a dispersive readout scheme for phase qubits [B3.4:1] using a capacitively shunted dc SQUID that avoids switching to the normal state. Instead of measuring the switching current, the change of the Josephson inductance of the SQUID is used to detect the qubit state. Depending on the flux state of the qubit, the resonance frequency of around 2 GHz is shifted by approximately 20 MHz, which corresponds to several line widths (Fig. 1). This shift is then detected by measuring the amplitude and phase of a microwave pulse reflected from the circuit.

Depending on the applied microwave power, the resonator can be operated in the linear or nonlinear regime. The nonlinear regime makes the extremely sensitive bifurcation readout possible, which allows for an even weaker coupling between the qubit and the detector in order to further reduce back-action. In this regime, it may also be possible to perform a direct readout of phase qubits that does not destroy the quantum state.

To test the readout system, we measured coherent (Rabi-) oscillations of the qubit (Fig. 2, left). It was found that the coherence time of the qubit was not limited by the readout, as the same qubit measured with conventional readout yielded a very similar energy relaxation time T1.

Currently, flux qubits show longer coherence times than phase qubits. In their case, the readout can be a limiting factor of coherence. In [B3.4:2], the dispersive readout of flux qubits through a transmission-line resonator (Fig. 2, right) in the intermediate coupling regime was demonstrated. In this regime, the resonator-qubit coupling is comparable to the dephasing rate of the qubit, thus the
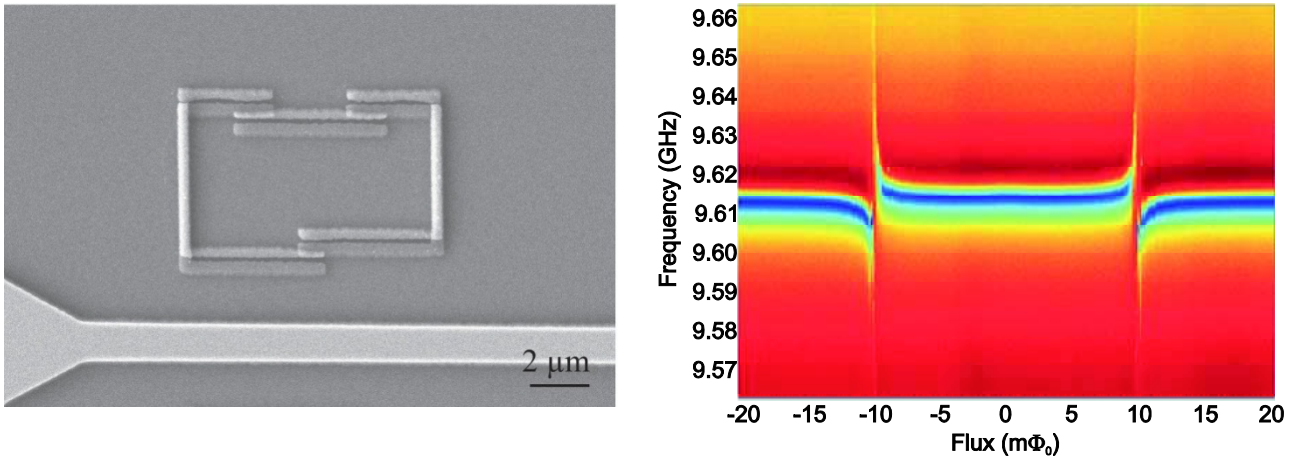
Figure 2: (left) SEM micrograph of a three-junction flux qubit coupled to a transmission-line resonator. (right) Dispersive shift of a resonator coupled to a flux qubit in the ground state. At ± 10 mΦ_0 the qubit and resonator frequencies match, revealing a level anti-crossing.

coupling does not introduce excessive extra decoherence.

The losses in resonators used in quantum circuits are of particular importance, because they directly influence the qubit coherence times. We studied losses in coplanar waveguide resonators in order to find the optimal conditions for quantum measurements. Samples with different superconductor and substrate materials were manufactured and their power and temperature dependent loss rates were compared.

2. Scalable Multiplexing Qubit Readout

Frequency-selective readout for superconducting qubits opens way towards scaling qubit circuits up to a large number of devices without increasing the number of measurement lines. The most recent achievement of this project is that we have demonstrated the readout of an array of 7 flux qubits located on the same chip. Each qubit is located near an individual quarter-wavelength resonator and is coupled to a single high-frequency transmission line. We performed spectroscopy of all 7 qubits and determined their parameters in a single measurement run.

Previous implementations of readout systems for superconducting qubits were not scalable beyond more than 2-3 devices. Conventional switching current measurements require a pair of current and voltage lines from the lowest temperature stage of the experiment to room temperature and dedicated electronics for each qubit. Readout of multiple qubits through a single transmission-type resonator has been demonstrated for up to three transmon qubits, but fails to scale because the readout channels for individual qubits are not independent.

Such independent channels can be provided by coupling a separate readout resonator to each qubit. These resonators can be designed to have slightly different resonance frequencies and can be fed through a single high-frequency line. If they are absorption-coupled, each resonator will act as a notch filter tuned by its qubit, and by measuring transmission through the feed-line at different frequencies, the state of each qubit can be determined independently.

We designed this readout scheme and implemented it for an array of 7 flux qubits [B3.4:5]. Each qubit is situated in the current antinode of a quarter-wave transmission-line resonator and all

resonators are coupled to a common microwave line. Using only this line and an external coil to tune the qubit transition frequencies, spectroscopy of all 7 qubits was performed (Fig. 3). On some of the qubits time-resolved measurements were also conducted in the same setup, providing information about relaxation and coherence times of the devices. Apart from multi-qubit systems, the fact that the parameters of many devices can be determined in a single cryostat run is useful for optimizing manufacturing processes.
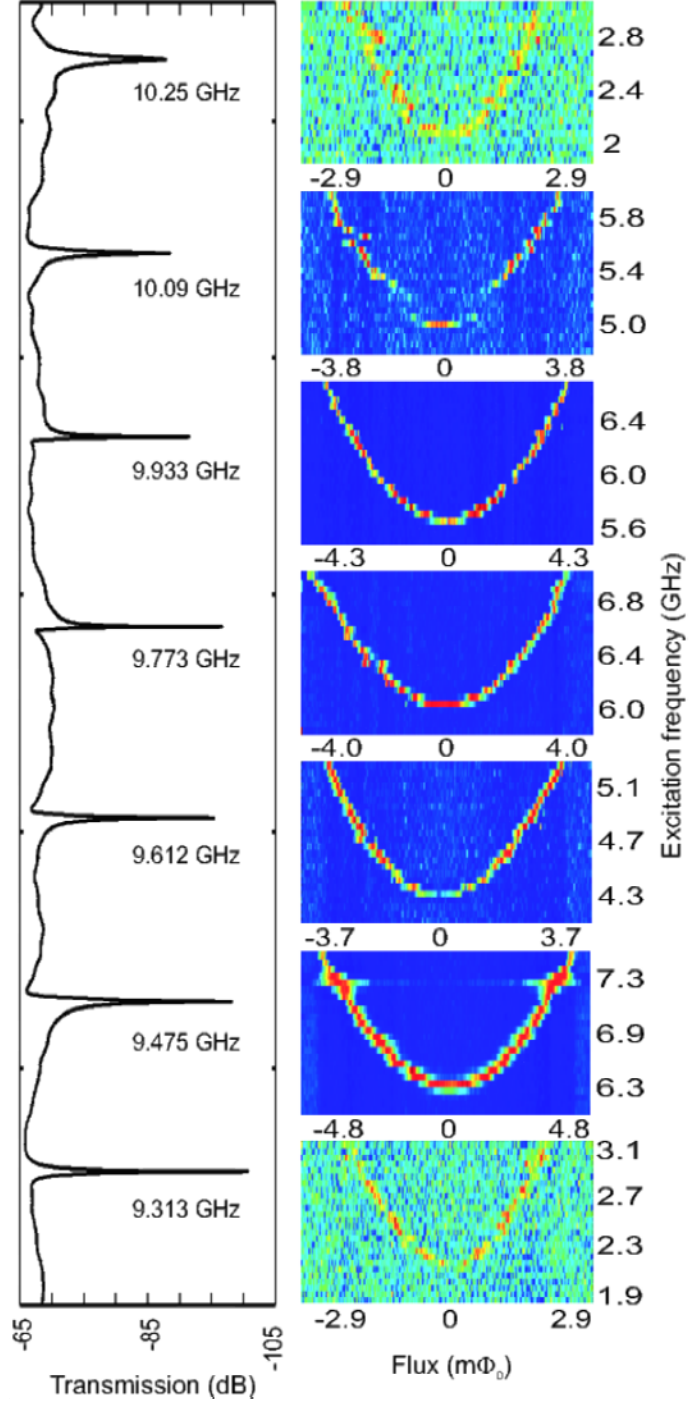

Fig. 3: (left) Transmission spectrum of the readout resonators and (right) spectroscopy of 7 flux qubits located on the same chip.

3. Development of Wideband Cryogenic Readout Amplifiers

When measuring quantum detectors, one regularly has to deal with extremely low-powered output signals. In the case of a qubit, any measurement disturbs its quantum state, with the rate of disturbance being proportional to the amplitude of the probe signal. Therefore, one typically works in the so-called single photon regime, where the average energy stored in the readout resonator is comparable to the energy a single photon at the resonator frequency.

3.1 Cryogenic Hybrid Readout Amplifiers

To introduce as little extra noise as possible to the output signal, cryogenic low-noise amplifiers are used which were developed in the past. The challenge here is the combination between the low power consumption operation regime, high gain, large bandwidth and low noise at 4.2 K. Commercial available amplifiers suffer at least at one of these requirements. The developed hybrid amplifiers ([B3.4:6]-[B3.4:8]) were now characterized in respect of their noise temperature. The introduced and established setup by [1] was used to determine the noise temperature of the two-stage hybrid amplifier. The results are shown in Fig. 4. The noise temperature within 8 GHz bandwidth results in $T_N \approx 60$ K. The hybrid cryogenic amplifiers were not only successfully used in project B3.4 but also in B1.5.

3.2 Development of Monolithic Microwave Integrated Circuits

Based on the hybrid cryogenic readout amplifiers with commercially available p-HEMTs (high electron mobility transistors) developed as high-speed interface [B3.4:6]-[B3.4:8], the main focus was a further decrease of the overall size and an increase of the achieved performance at the same time.The collaboration with the IAF (Fraunhofer Institute for Applied Solid State Physics, Freiburg) allowed the application of the integrated metamorphic HEMT technology with a gate length of 100 nm.
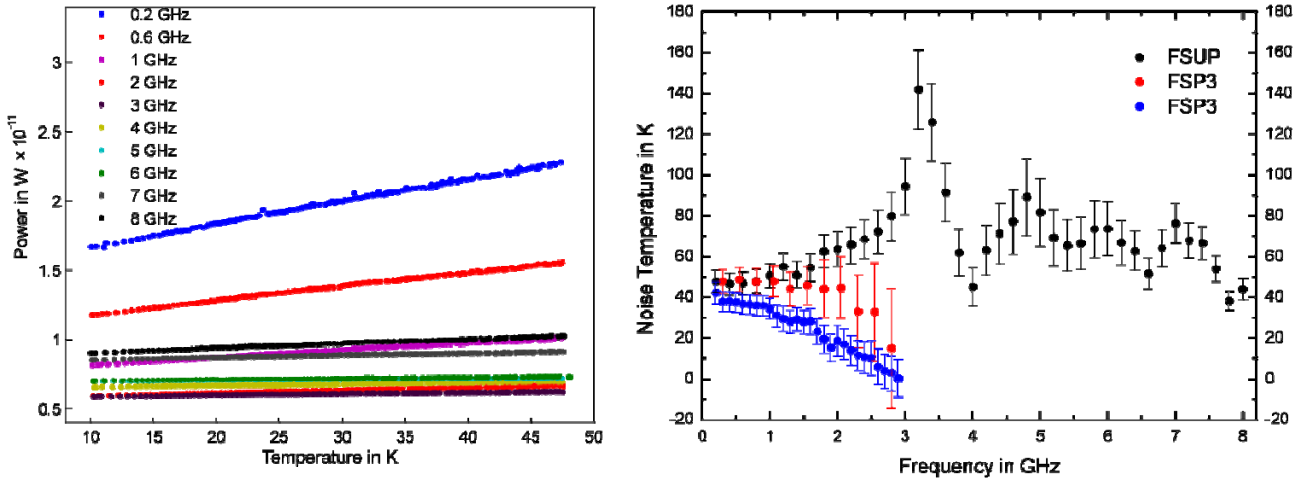

Fig. 4:Output power vs. temperature of the two-stage hybrid amplifier for different single frequencies (right) and the calculated noise temperature of the two stage hybrid amplifier vs. bandwidth (left). The limited bandwidth of 8 GHz belongs to the setup.

This technology features a maximum cutoff frequency f_T of 220 GHz and f_{max} of 300 GHz and is featuring a state of the art low noise performance at room temperature as well as at cryogenic temperatures [2], [3] with a corresponding circuit design.

The transmission lines were realized in a coplanar waveguide design and included the passive elements, e.g. thin film resistors (NiCr), capacitors (SiN dielectric layer) and spiral inductors. Typical drain currents at ambient temperature for low noise amplifiers realized in this technology are 150 mA/mm. A common source transistor circuit with the previously described technology was selected to achieve the challenging bandwidth requirements in combination with a low noise figure. A specific noise-matching circuitry at the amplifier input was neglected because the usage of any noise-matching inductances added an unwanted distortion of the original output signal. The voltage signal gain of about 20 dB could be realized by an amplifier with three stages. Two different amplifiers were designed in respect to the selected load impedances. Version A used resistors at the drain and had a cut-off frequency at the lower frequency side of 0.3 GHz. The main disadvantage of these resistors is the increased power consumption up to 90 mW at room temperature. Therefore the resistors were replaced by on-chip inductors in version B, which cutted the power consumption by a factor of 2, but increased the lower frequency side up to 1.3 GHz. In both versions of the amplifier, a resistive load was used to increase the stability of the circuits. Thus, unconditional stability could be achieved for both amplifier versions. The micrographs of both fabricated MMICs are exemplarily depicted in Fig. 5. Both MMICs were realized on a size of 3 x 1.5 mm² [B3.4:3].

On-chip measurements of the scattering parameters were performed with an appropriate DC bias and RF probes. The measurements were performed at room temperature and 7.2 K in a liquid-free cryostat. After the room temperature measurements, the amplifier versions were cooled down to 7.2 K within the liquid-free cryostat. The achieved values for the scattering parameters are depicted in Fig. 6 for the amplifier version A and version B. The focus of these experiments was the behavior of the gain $|S_{21}|$ by decreasing temperature and available power consumption. The reflection coefficients were totally unaffected by the variation of these two parameters in both designs. With almost the same power consumption as room temperature, the gain increased constant 5 dB over the whole bandwidth of 25 GHz. If the power consumption wasdecreased to 22 mW, the performance of the gain reduced as expected, but almost the same frequency behavior over the whole bandwidth ($|S_{21}| > 5$ dB) could be observed. Compared to thedeveloped hybrid amplifiers [B3.4:6]-[B3.4:8],
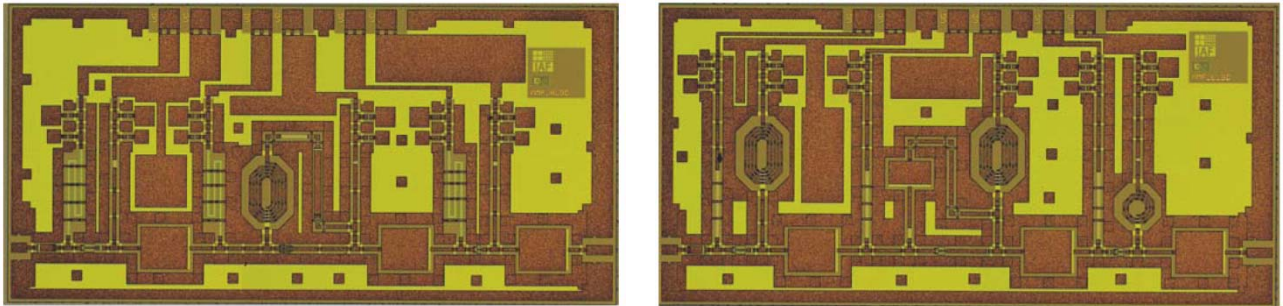

Fig.5:Micrographs of the fabricated MMICs with drain resistors (version A, left) and inductive load impedances (version B, right).

the power consumption is larger by a factor of 3 but achieved a clearly larger bandwidth (factor 2). Also, amplifier version B showed at lower power consumption, compared to room temperature, the same frequency behavior of $|S_{21}|$. The gain was slightly decreased ($|S_{21}| = 20$dB) but the bandwidth with a flat gain was still about 4 GHz. By reducing the power consumption to 9.5 mW, which is in the range of the hybrid amplifiers, the gain lost at least 5 dB over the whole bandwidth. Thus, the available bandwidth with flat gain and $|S_{21}| > 10$ dB is reduced to 2 GHz. The total useful bandwidth is limited by $|S_{21}| = 0$ dB at 11 GHz.

For the usage in a detector system, the MMICs had to be mounted in an appropriate microwave housing. The interface between the detector at the input side and the room temperature electronic at the output side was realized by SMA connectors. The first developed gold-coated brass housing had a size of 33 × 40.6 mm² and is depicted in Fig. 7. The RF connection with the MMIC was realized by a coplanar transmission line with a linewidth of 50 μm and gap of 30 μm at each side. This cross-section allowed a direct bonding between the MMIC and the transmission lines. To mount the

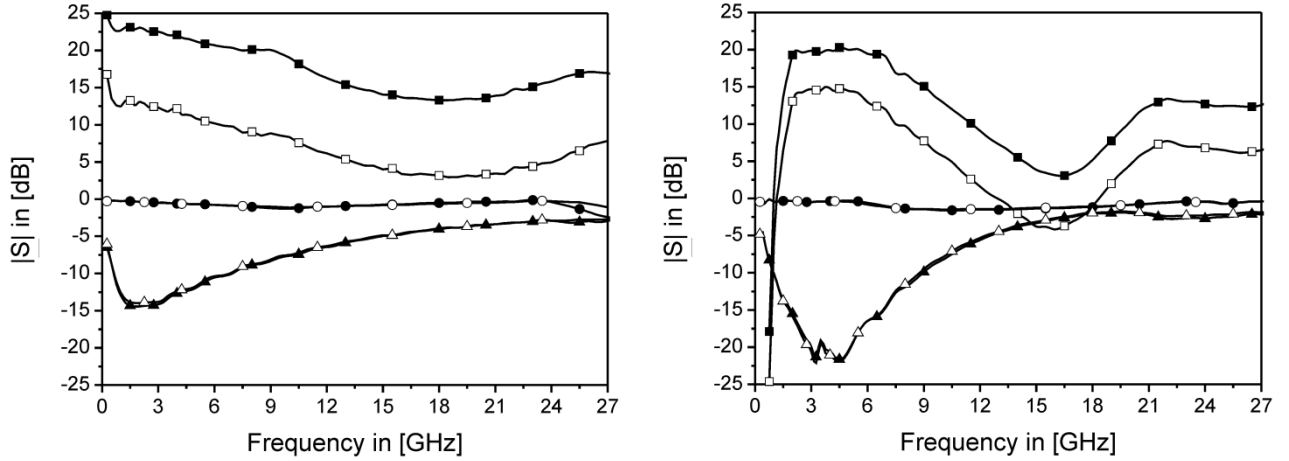Fig. 6:On-chip measurement results of the scattering parameters $|\underline{S}_{21}|$ (—■—), $|\underline{S}_{11}|$ (—●—) and $|\underline{S}_{22}|$ (—▲—) for the version A (left) with a total power consumption of $P_V = 90$ mW at 7.2 K. By reducing the power consumption to 22 mW, the gain $|\underline{S}_{21}|$ (—□—) decreases by 10 dB while the reflection coefficients $|\underline{S}_{11}|$ (—○—) and $|\underline{S}_{22}|$ (—△—) were almost constant. Measurement results of the scattering parameters for version B (right) with a total power consumption of $P_V = 24.5$ mW at 7.2 K. By reducing the power consumption to 9.5 mW, the gain $|\underline{S}_{21}|$ decreases by 5 dB while the reflection coefficients were also almost constant.

Fig.7: Micrograph of the housed MMIC. The size of the gold-coated brass housing is 33 × 40.6 mm². The connection with the external electrical network is realized by two SMA connectors.

SMA connector, the coplanar line has a taper with an increased linewidth of 500 μm and gap of 200 μm. Thus, a 50 Ω matched RF feed is supported. The DC bias was supplied by feed-through PI filters into the housing which were then soldered on a Rogers TMM10i substrate printed circuit

board (PCB). To match the small MMIC pads (100 × 100 μm²) a thin film spider-web was placed between the PCB and the MMIC. The DC bias for all 3 gate and drain voltages were finally bonded. First DC measurements were successfully realized while the cryogenic characterization is under progress [B3.4:3].

4. Optimization of Multi-pixel Detector Systems

While the operating principle of a frequency-division multiplexing detector system is straightforward, the actual implementation of such detectors is challenging. As the detection bandwidth is always limited, the frequencies of individual pixels should be as close as possible, but still separable. Thus the development of large detector arrays requires an intimate knowledge of their mode of operation in respect of the microwave regime [B3.4:9].
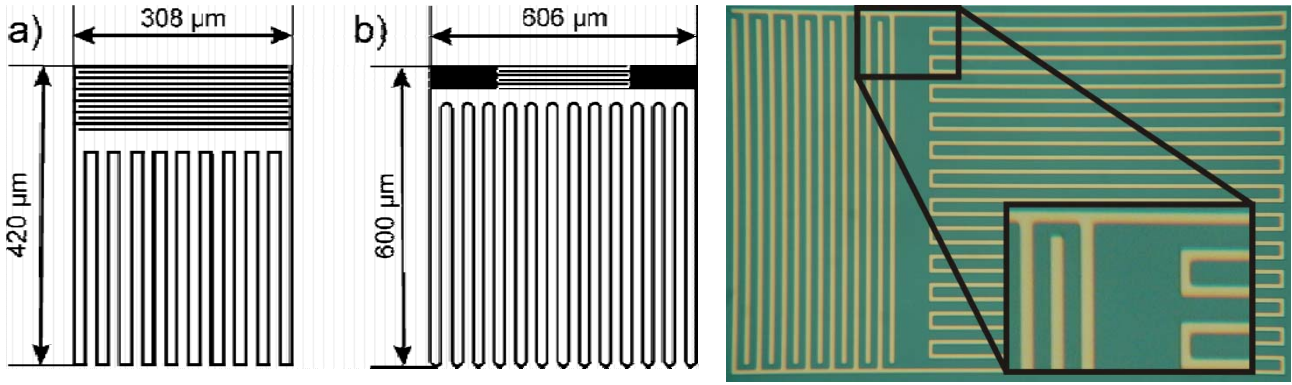
Figure 8.(left) Sketch of the two footprints for the investigated LEKID structures. The size of the footprints was 420 × 300 μm² for (a) and 600 × 600 μm² for (b), respectively.(right) Micrograph of a fabricated LEKID structure in niobium.
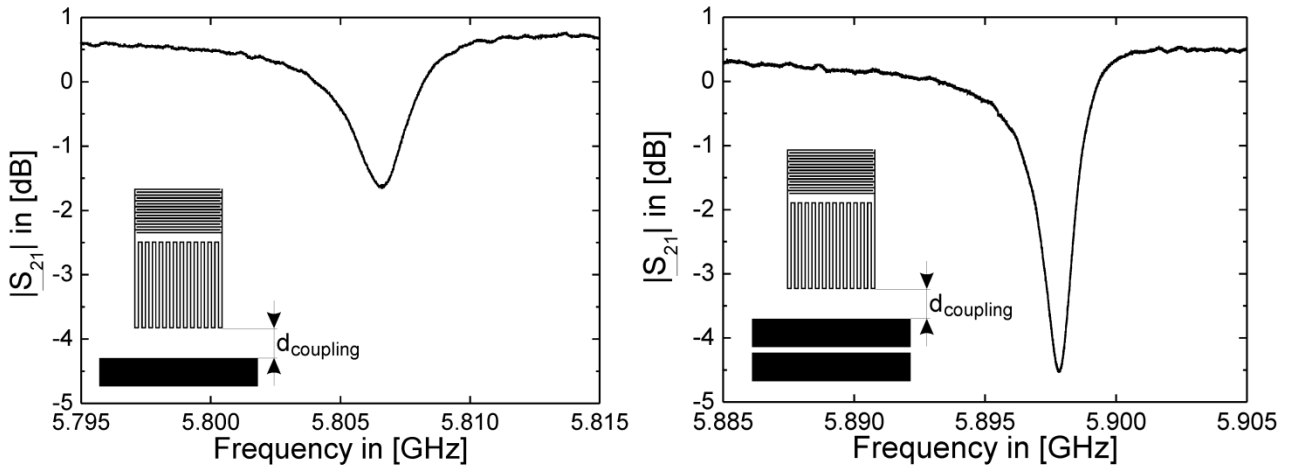
Fig.9: Measurement results of identical LEKID structures coupled to different feed-lines at 4.2 K. The unloaded quality factor could be increased by a factor of 2 with selecting a coplanar strip line (right) instead of a microstrip line (left). All microwave parameters like coupling distance were identical during measurements. The positive offset of the transmission coefficient $|\underline{S}_{21}|$ in both graphs was caused by the calibration at room temperature and the inset shows the orientation of the LEKID in respect to the MS/CPS lines.

We studied the coupling of lumped element resonators (Fig. 8) used as kinetic inductance detectors to different feed-lines [B3.4:4].Different microwave parameters, like the coupling distance between the resonators and the feed-line, the transmission line technique for the feed-line itself and the orientation of the resonator with respect to the feed-line were varied. It was found that, while a microstrip design offers free wiring to the designer and therefore a large potential for arrays with a high packing density, the required ground plane at the back of the chip limits achievable quality factors and complicates the prediction of the resonance frequencies by introducing parasitic
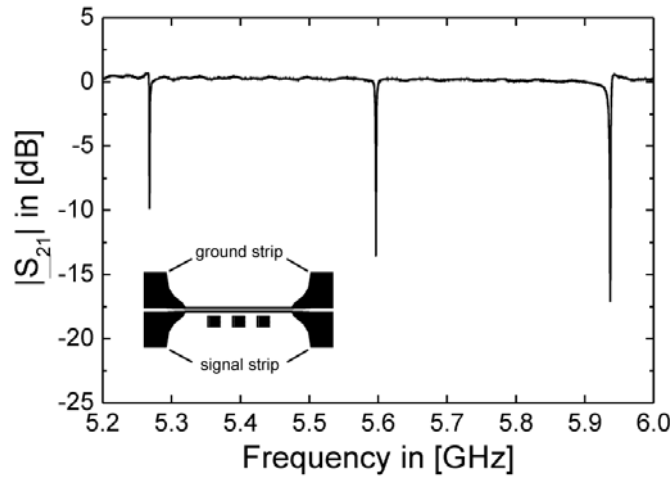

Fig. 10: Measurement result of a 3-pixel array with large LEKID structures coupled perpendicular to a coplanar strip line at the signal strip side. The coupling distance was in all 3 cases 80 μm. The positive offset of the transmission coefficient $|\underline{S}_{21}|$ was caused by the calibration at room temperature and the inset shows the orientation and arrangement of the 3 LEKIDs in respect to the CPS line.

capacitances. The elimination of these parasitic effects was realized by an alternative transmission line technique, namely the coplanar stripline. In Fig. 9 this comparison is distinguishable.

In the latter configuration, unloaded quality factors of up to 13,000 were realized at the cost of a slightly reduced physical packing density and first multi-pixel devices up to a number of 3 were designed, fabricated and measured. The measurement results are shown in fig. 11. At mK temperatures the unloaded quality factor should increase by a factor of about 5 and therefore a smaller frequency spacing could be introduced which should lead to the required high packaging density.

References
- own work with complete titles -

[1]   C. Schwemmer, T. Wirth, A. Lukashenko, J. Lisenfeld, M. Mück and A. Ustinov, *Noise Measurements of Cryogenic Amplifiers for Qubit Experiments*, DPG Jahrestagung und DPG Frühjahrstagung des AKF, Dresden (2009).
[2] M. Schlechtweg, A. Tessmann, A. Leuther, C. Schwörer, H. Massler, M. Mikulla, M. Walther, and R. Lösch, Proceedings physica status solidi c, (c) 3, no. 3, pp.465-468, 2006.
[3] A. Leuther, A. Tessmann, I. Kallfass, R. Lösch, M. Seelmann-Eggebert, N. Wadefalk, F. Schäfer, J.D. GallegoPuvol, M. Schlechtweg, M. Mikulla, O. Ambacher, Indium Phosphide & Related Materials, 2009. IPRM '09. IEEE International Conference on, pp. 188-191 May 2009.